ROZPRAWY INŻYNIERSKIE • ENGINEERING TRANSACTIONS • 29, 3, 351—369, 1981
Polska Akademia Nauk • Instytut Podstawowych Problemów Techniki

NUMERICAL CALCULATION OF PRESSURE LOSS AND FORCED CONVECTIVE HEAT TRANSFER IN ROTATING CHANNELS OF ARBITRARY RECTANGULAR CROSS SECTION

R. SCHILLING (KARLSRUHE)

The steady fully-developed laminar flow field and temperature field in rotating straight rectangular channels is investigated by a finite difference method. The solution of the Navier–Stokes equations and the energy equation yields the pressure loss, heat transfer and the efficiency factor as a function of the Reynolds number, Rotation number and aspect ratio. The numerical results agree well with available experimental data.

NOMENCLATURE

Dimensional	*Nondimensional*	Meaning,
a, b		width and height of the channel,
	A_0—A_5	coefficients,
c		heat capacity,
c_p, c_t	C_p, C_θ	pressure and temperature gradient,
d_h	D	hydraulic diameter,
	De	Dean number,
	Ec	Eckert number,
	F	dummy variable,
	$F_{cp}, F_{c\theta}$	numerical errors,
	$G\ddot{u}$	efficiency factor,
	K_p, K_θ	pressure and temperature gradient obtained from the control equations,
	Nu	Nusselt number,
	NY, NZ	number of divisions in Y– and Z–directions,
p	P	static pressure,
	Pr	Prandtl number,
	Re	Reynolds number,
	Ro	Rotation number,
	Ta	Taylor number,
u, v, w	U, V, W	Relative velocity components,
x, y, z	X, Y, Z	Cartesian coordinates,
β		heat conductivity,
	λ	aspect ratio,
ν		kinematic viscosity,
ρ		density
	ζ	friction factor,

ω_0		angular velocity,
ξ	Ω	vorticity function,
ψ	Ψ	stream function,
t	θ	temperature.

Subscripts

j, k	space subscript
m	average value
w	wall
*	reduced value
0	value for nonrotating channels

1. Introduction

In industrial equipment helically-coiled ducts rotating around their axis can be used as heat exchangers (Fig. 1). The flow through a curved rotating channel is characterized by the centrifugal and Coriolis forces which cause a pressure gradient normal to the main flow direction coupled with the main velocity profile. These additional body forces are unbalanced near the wall and therefore cause the well--known double helix secondary flow in a cross section of the channel. The onset of secondary flow yields to an increase of the flow resistance as well as of the heat

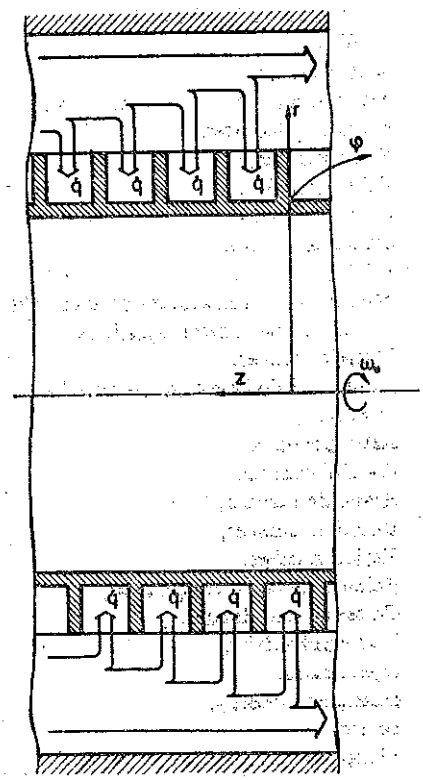

Fig. 1. Design of a rotating heat exchanger.

transfer compared with the flow in a straight nonrotating channel. Furthermore the onset of turbulence is inhibited so that the critical Reynolds number may increase from $Re_{crit}=2.000$ up to 20.000 considering high rotation speed or strong curvature. Therefore laminar flow can be expected to reach high values of the Reynolds number. In spite of this essential simplification, either an analytical or a numerical solution is known. A lot of publications deal with the flow and heat transfer in curved or rotating channels having a square or circular cross sections. Generally the increase of pressure loss and heat transfer due to curvature or rotation was studied using the perturbation analysis boundary layers approximations or finite difference methods [1], ..., [8]. But there are only a few works dealing with the influence of the aspect ratio. For example, CHENG *et al.* [3] and [7] have calculated the flow and heat transfer in curved rectangular channels for various aspect ratios. But systematic numerical investigations have not been carried out. In the case of rotating channels, however, this influence has not yet been studied.

2. FORMULATION OF THE PROBLEM

The purpose of this work is to present an accurate numerical solution assuming small curvature and constant physical properties of the fluid and neglecting viscous heating. If the hydraulic diameter d_h is small compared with the axial length of the channel and with the radius of curvature, the influence of inlet flow and the effect of curvature may be neglected. If we suppose furthermore an axially uniform heat flux at the wall and zero heat flux at the remaining walls, a hydrodynamically and thermally fully-developed laminar flow through a rotating straight channel is considered.

Taking a Cartesian coordinate system rotating around its z-axis with constant angular velocity ω_0, the relative velocity components are u in the x, v in the y and w in the z-direction, where x is the main flow direction (see Fig. 2). The dimensions a and b mean the width and height of the channel, respectively.

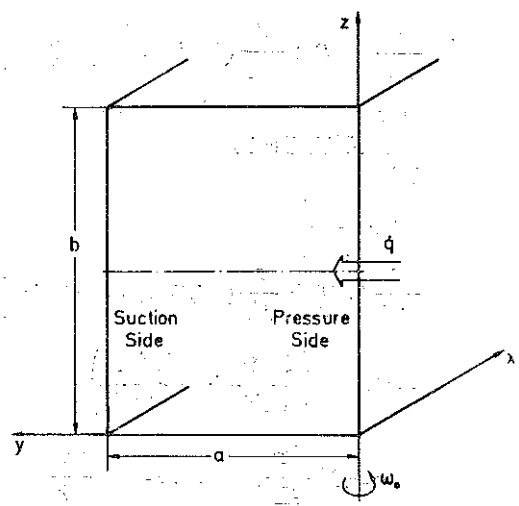

FIG. 2. Geometry of the channel and rotating coordinate system.

Because the Coriolis forces cause a decrease of the static pressure in the positive y-direction the walls at $y=0$ and $y=a$ may be defined as the pressure and suction side (PS and SS) of the channel respectively. The influence of centrifugal forces due to rotation can be eliminated introducing a reduced pressure $p^*=p-\rho/2\omega_0^2\,(x^2+y^2)$. Since there are no additional body forces acting in the z-direction, the flow and temperature field is symmetric to the line $z=b/2$.

2.1. Governing equations

The governing equations describing the fluid flow and heat transfer problem are the Navier-Stokes equations, the continuity and energy equation. Considering the assumptions stated above, it is convenient to introduce a stream function ψ which satisfies the continuity equation and a vorticity function ξ in order to eliminate the pressure terms from the secondary flow equations. Using the following nondimensional quantities

$$X=\frac{x}{d_h}\frac{1}{\mathrm{Re}},\qquad Y=\frac{y}{a},\qquad Z=\frac{z}{b},\qquad \lambda=\frac{a}{b},$$

$$U=\frac{u}{u_m},\qquad V=\frac{v}{u_m}\mathrm{Re}\frac{d_h}{a},\qquad W=\frac{w}{u_m}\mathrm{Re}\frac{d_h}{b},\qquad C_p=\frac{c_p\,d_h}{\rho u_m^2}\mathrm{Re},$$

$$\Omega=\xi\frac{d_h}{u_m}\mathrm{Re}\frac{a}{b},\qquad \Psi=\frac{\psi}{u_m\,d_h}\mathrm{Re}\frac{a}{b},\qquad \theta=\frac{t_w-t}{t_w-t_m}\frac{1}{C_\theta},\qquad C_\theta=\frac{c_t\,d_h}{t_w-t_m}\mathrm{Re},$$

one obtains a set of four elliptic partial differential equations in conservation form and two additional equations for evaluating the pressure and temperature gradient. The secondary flow velocities may be expressed in terms of the stream function.

Governing equations

Main flow

$$\frac{\partial}{\partial Y}(VU)+\frac{\partial}{\partial Z}(WU)=-C_p+2\,\mathrm{Ro}\,V+D^2\left(\frac{\partial^2 U}{\partial Y^2}+\lambda^2\frac{\partial^2 U}{\partial Z^2}\right),$$

(2.1)

$$\int_0^1\int_0^1 U\,dY\,dZ\equiv 1.$$

Secondary flow

$$\frac{\partial}{\partial Y}(V\Omega)+\frac{\partial}{\partial Z}(W\Omega)=2De^2\,D^2\,\lambda^2\frac{\partial U}{\partial Z}+D^2\left(\frac{\partial^2\Omega}{\partial Y^2}+\lambda^2\frac{\partial^2\Omega}{\partial Z^2}\right),$$

(2.2)

$$-\Omega=D^2\left(\frac{\partial^2\Psi}{\partial Y^2}+\lambda^2\frac{\partial^2\Psi}{\partial Z^2}\right),$$

$$V=D^2\frac{\partial\Psi}{\partial Z},\qquad W=-D^2\frac{\partial\Psi}{\partial Y}.$$

Temperature field

$$\frac{\partial}{\partial Y}(V\theta)+\frac{\partial}{\partial Z}(W\theta)=U, \quad +\frac{D^2}{\mathrm{Pr}}\left(\frac{\partial^2\theta}{\partial Y^2}+\lambda^2\frac{\partial^2\theta}{\partial Z^2}\right),$$

(2.3)

$$C_\theta=\frac{1}{\int_0^1\int_0^1\theta dY\,dZ}.$$

The following boundary conditions are assumed

Flow field

$$Y=0 \quad \text{and} \quad Y=1: \quad U=V=W=\Psi=0, \quad \Omega=-D^2\frac{\partial^2\Psi}{\partial Y^2};$$

$$Z=0: \quad U=V=W=\Psi=0, \quad \Omega=-D^2\lambda^2\frac{\partial^2\Psi}{\partial Z^2};$$

$$Z=\frac{1}{2}: \quad W=\Omega=\Psi=0, \quad \frac{\partial}{\partial Z}(U,V)=0.$$

Temperature field

heat transfer at pressure side

$$Y=0: \quad \theta=0; \quad Y=1: \quad \frac{\partial\theta}{\partial Y}=0;$$

heat transfer at suction side

$$Y=0: \quad \frac{\partial\theta}{\partial Y}=0; \quad Y=1: \quad \theta=0;$$

$$Z=0 \quad \text{and} \quad Z=\frac{1}{2}: \quad \frac{\partial\theta}{\partial Z}=0.$$

The parameters characterizing this problem are

$\mathrm{Re}=\dfrac{u_m d_h}{\nu}$ Reynolds number,

$\mathrm{Ro}=\dfrac{\omega_0 a}{u_m}$ rotation number,

$\lambda=\dfrac{a}{b}$ aspect ratio,

$D=\dfrac{d_h}{a}=\dfrac{2}{1+\lambda}$ relative hydraulic diameter,

$\mathrm{Pr}=\dfrac{\rho\nu c}{\beta}$ Prandtl number.

The governing equations, however, point out that the Reynolds number does not occur as a single parameter but is connected with the square root of the Rotation number. Following the analogy between the flow in curved and rotating ducts, s. TREFETHEN [9], this parameter may be defined as a modified Dean number

$$\mathrm{De}=\mathrm{Re}\sqrt{\mathrm{Ro}}. \tag{2.4}$$

The numerical solution yields the flow and the temperature field data as a function of the pertinent parameters:

flow field

$$U, V, W, C_p=f(\mathrm{De}, \mathrm{Ro}, \lambda); \tag{2.5}$$

temperature field

$$\theta, C_\theta=F(\mathrm{De}, \mathrm{Ro}, \lambda, \mathrm{Pr}).$$

After having calculated the pressure gradient C_p and temperature gradient C_θ the friction factor ζ, the Nusselt number Nu and the efficiency factor *Gü* can be evaluated using the following relationships:

$$\zeta=\frac{2}{\mathrm{Re}}C_p,$$

$$\mathrm{Nu}=\frac{\mathrm{Pr}}{D^2}C_\theta, \tag{2.6}$$

$$G\ddot{u}=\frac{C_\theta}{C_p}\cdot\frac{1}{Ec}, \qquad Ec=\frac{u_m^2}{c\,(t_w-t_m)}.$$

2.2. Control equations

Integrating the axial momentum equation and the energy equation over the corss section of the channel, two control equations may be deduced to check the accuracy of the numerical solution

$$C_p\approx K_p, \tag{2.7}$$

where

$$K_p=D^2\left\{\int_0^1\left[\left.\frac{\partial U}{\partial Y}\right|_{Y=1}-\left.\frac{\partial U}{\partial Y}\right|_{Y=0}\right]dZ-2\int_0^1\left.\frac{\partial U}{\partial Z}\right|_{Z=0}dZ\right\};$$

$$C_\theta\approx K_\theta, \tag{2.8}$$

where

$$K_\theta=\frac{D^2}{\mathrm{Pr}}\int_0^1\left\{\left.\frac{\partial\theta}{\partial Y}\right|_{Y=1}-\left.\frac{\partial\theta}{\partial Y}\right|_{Y=0}\right\}dZ.$$

Equations (2.7) and (2.8) show that the conservation of momentum and energy is to be satisfied respectively. Hence the numerical errors can be evaluated from the following relationships:

$$F_{C_p}=\frac{C_p-K_p}{C_p}, \qquad F_{C_\theta}=1+K_\theta. \tag{2.9}$$

The numerical errors of the axial momentum equation and energy equation primary depend on the mesh sizes $\Delta Y=1/NY$ and $\Delta Z=0.5/NZ$ and secondary on the pertinent parameters.

$$\begin{aligned} F_{C_p}&=f(NY, NZ, \mathrm{De}, \mathrm{Ro}, \lambda),\\ F_{C_\theta}&=f(NY, NZ, \mathrm{De}, \mathrm{Ro}, \lambda, P),\end{aligned} \tag{2.10}$$

where NY and NZ are the number of divisions in the Y- and Z-direction respectively for one half of the cross section.

2.3. *Numerical solution*

The elliptic partial differential equations were solved using a second-order finite difference scheme with central difference approximations for the convective and diffusive terms as

$$\begin{aligned} \left.\frac{\partial F}{\partial Y}\right|_{j,k}&=\frac{F_{j+1,k}-F_{j-1,k}}{2\Delta Y}+O(\Delta Y^2),\\ \left.\frac{\partial^2 F}{\partial Y^2}\right|_{j,k}&=\frac{F_{j+1,k}-2F_{j,k}+F_{j-1,k}}{\Delta Y^2}+O(\Delta Y^2)\end{aligned} \tag{2.11}$$

and a three point formula for the wall vorticity as

$$\Omega_W=-\frac{-7\Psi_W+8\Psi_{W-1}-\Psi_{W-2}}{2\Delta Y^2}+O(\Delta Y^2). \tag{2.12}$$

Substituting the spatial derivatives of the differential equations by the corresponding finite difference approximations, one obtains a set of four difference equations in the following form:

$$A_1 F_{j-1,k}+A_0 F_{j,k}+A_2 F_{j+1,k}+A_3 F_{j,k-1}+A_4 F_{j,k+1}=A_5, \tag{2.13}$$

where the coefficient A_0 is constant and the coefficients A_1–A_5 are functions of Y, Z and j, k respectively. For example, considering the axial momentum equation $(2.1)_1$, the coefficients A_0–A_5 may be written as follows:

$$\begin{aligned} A_0&=-2\left\{\left(\frac{\Delta Z}{\lambda\Delta Y}\right)^2+1\right\},\\ A_1&=\left(\frac{\Delta Y}{2}V_{j-1,k}\frac{1}{D^2}+1\right)\left(\frac{\Delta Z}{\lambda\Delta Y}\right)^2,\\ A_2&=\left(-\frac{\Delta Y}{2}V_{j+1,k}\frac{1}{D^2}+1\right)\left(\frac{\Delta Z}{\lambda\Delta Y}\right)^2,\\ A_3&=\frac{\Delta Z}{2}W_{j,k-1}\frac{1}{D^2\lambda^2}+1,\\ A_4&=-\frac{\Delta Z}{2}W_{j,k+1}\frac{1}{D^2\lambda^2}+1,\\ A_5&=(C_p-2\,\mathrm{Ro}\,V_{j,k})\left(\frac{\Delta Z}{D\lambda}\right)^2.\end{aligned} \tag{2.14}$$

The difference equations were solved iteratively using Gaussian elimination on the lines

$$\begin{aligned} Z, k=\text{const}: &\quad A_1 F_{j-1,k}+A_0 F_{j,k}+A_2 F_{j+1,k}=A_5^*, \\ Y, j=\text{const}: &\quad A_3 F_{j,k-1}+A_0 F_{j,k}+A_4 F_{j,k+1}=A_5^{**} \end{aligned} \tag{2.15}$$

with successive over or under relaxation. The modified coefficients A_5^* and A_5^{**} become

$$\begin{aligned} A_5^* &= A_5-(A_3 F_{j,k-1}+A_4 F_{j,k+1}), \\ A_5^{**} &= A_5-(A_1 F_{j-1,k}+A_2 F_{j+1,k}). \end{aligned} \tag{2.16}$$

The iterations were carried out with alternating direction and were terminated when a relative error criterion $\varepsilon=10^{-5}$ was satisfied.

3. Results

Starting the computations which were carried out on a 1108 UNIVAC computer of the "Rechenzentrum der Universität Karlsruhe", the first question to answer is how many mesh points $(NY+1)\times(NZ+1)$ are needed to obtain a sufficiently accurate solution. Therefore the influence of the number of mesh points on the pressure

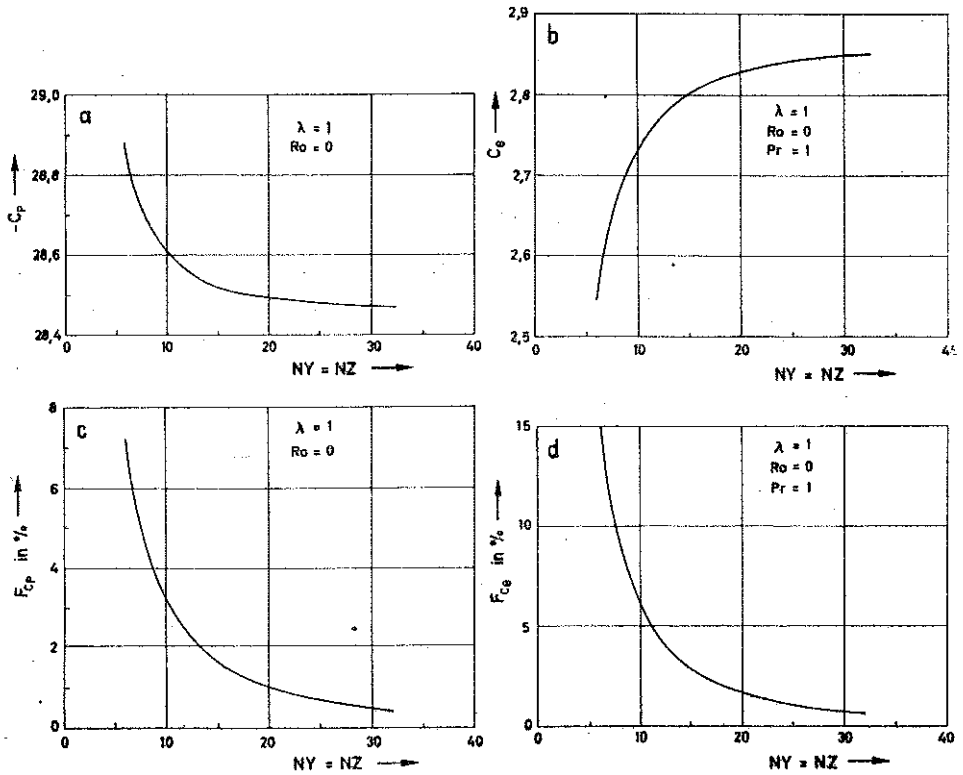

FIG. 3. Influence of number of mesh points on the pressure and temperature gradient C_p and C_θ as well as on the numerical errors F_{C_p} and F_{C_θ}.

and temperature gradient C_p and C_θ as well as on the numerical errors F_{C_p} and F_{C_θ} was studied assuming Ro=0, λ=1 and Pr=1. Furthermore the number of mesh points in the Y-and Z-direction was supposed to be equal considering one half of the cross section, $NY=NZ$. The computations show that the pressure and temperature gradients reach an asymptotic value each with an increasing number of mesh points while the numerical errors run to zero:

$$C_p\,(\mathrm{Ro}=0,\lambda=1)=C_{p_0}=-28.5,\qquad C_\theta\,(\mathrm{Ro}=0,\lambda=1)=C_{\theta_0}=2.85. \tag{3.1}$$

Based on these results all numerical calculations were carried out using 21×21 mesh points. Throughout this study the Prandtl number was held fixed at Pr=1 (Fig. 3).

3.1. Pressure loss

Evaluating the pressure losses in rotating channels the pressure gradient C_p or the friction factor ζ must be known. In Fig. 4 the friction factor ζ is plotted against the Reynolds number Re for the aspect ratio λ=1 with the Rotation number Ro as a parameter. For Ro=0 the numerical results yield the exact solution $\zeta=57/\mathrm{Re}$. Considering a constant value of Ro the friction factor decreases with increasing Re corresponding to the exact solution. At a critical value of Re the curve begins

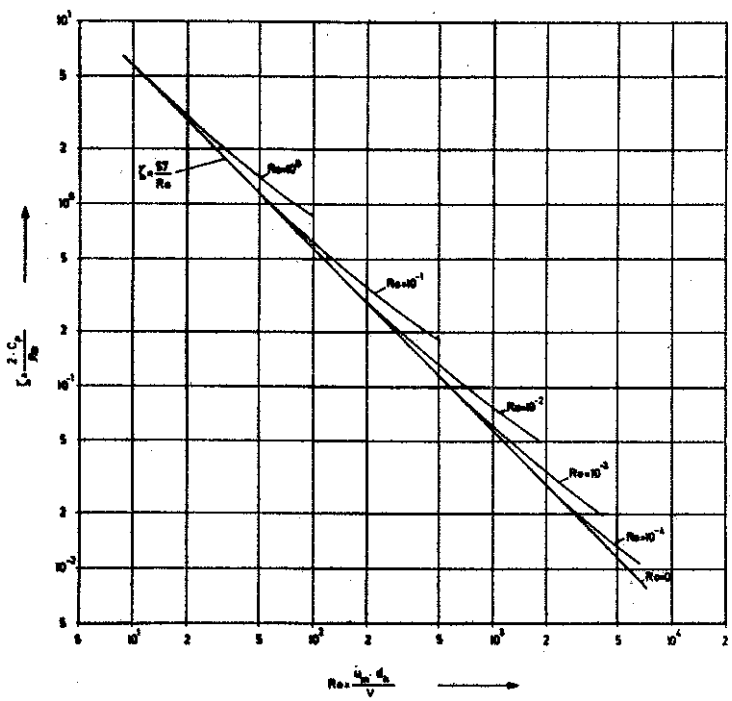

FIG. 4. Friction factor φ versus Reynolds number Re for λ=1 with Rotation number Ro as a parameter.

to vary up because the secondary flow strongly increases. This behaviour may be understood because the excitation of the secondary flow is proportional to the square of the Reynolds number.

Assuming constant values of angular velocity ω_0 and mean velocity of flow u_m, this graph shows the influence of viscosity ν on the friction factor. In order to show the influence of the mean velocity u_m supposing constant values of ω_0 and ν, the Taylor number $\mathrm{Ta}=\omega_0 a d_h/\nu$ which is the product of Re and Ro is to be held fixed. The friction factor ζ is plotted against the Reynolds number for $\lambda=1$ with the Taylor number Ta as a parameter (see Fig. 5).

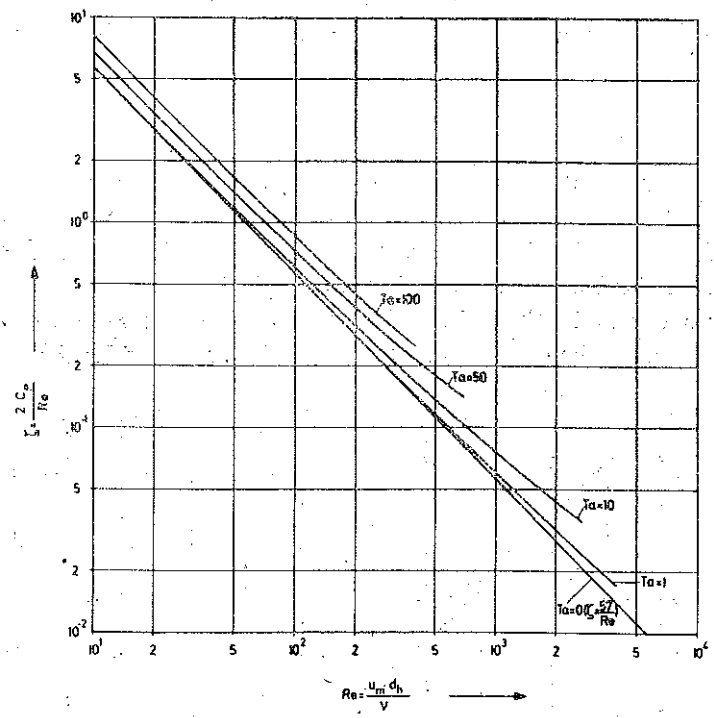

FIG. 5. Friction factor ζ versus Reynolds number Re for $\lambda=1$ with the Taylor number Ta as a parameter.

For $\mathrm{Ta}=0$, that means $\mathrm{Ro}=0$, we obtain again the exact solution $\zeta=57/\mathrm{Re}$. Considering Taylor numbers $\mathrm{Ta}>0$ the numerical solution yields parallel lines in the range of low and moderate Reynolds numbers. Similar to the case shown above the curves begin to vary up at larger values of Re because the excitation of secondary flow is proportional only to the first power of the Reynolds number.

The influence of rotation ω_0 is generally demonstrated correlating the increase of the pressure gradient or pressure loss to the Dean number De. In the case of small values of the Rotation number Ro the Dean number is the similarity parameter of this problem and all curves shown above coincide to a single curve (see Fig. 6).

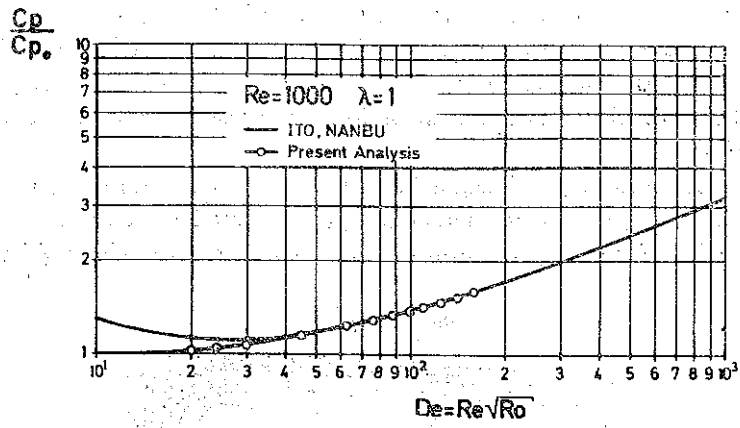

FIG. 6. Increase of pressure gradient C_p/C_{p_0} due to rotation versus Dean number for Re=1000 and $\lambda=1$.

For De>10 the pressure gradient C_p increases as the Rotation number and the secondary flow increases. In this case the excitation of the secondary flow motion is proportional to the Rotation number. In Fig. 6 the numerical solution is compared with the semi-empirical relationship of ITO, NANBU [10]. The comparison is found to be good. However, a semi-logarithmic plotting shows that the similarity is only valid up to the Rotation numbers Ro<0.10 (see Fig. 7). For Ro>0.10 the computed pressure gradients clearly deviate from the curve.

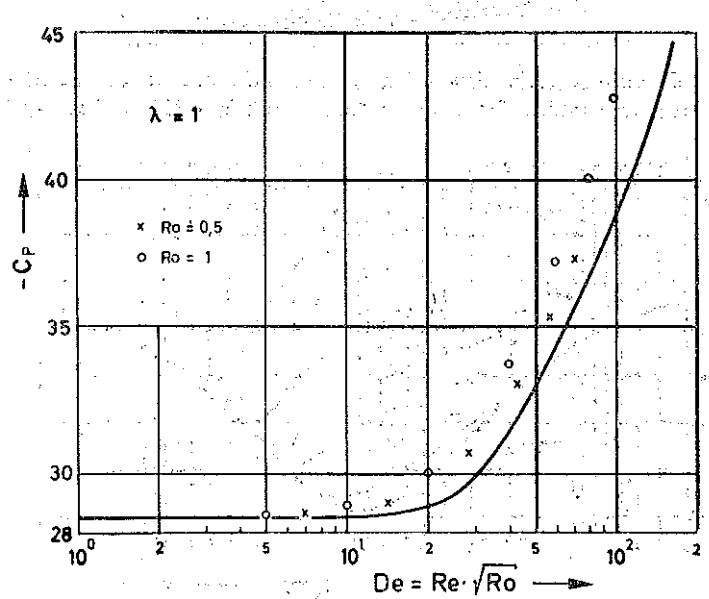

FIG. 7. Pressure gradient C_p versus Dean number De for $\lambda=1$ with Rotation number Ro as a parameter.

At a critical Dean number De$\approx$160 and Ro$\simeq 2.6 \cdot 10^{-2}$ a second pair of counter-rotating vortices appears (see Fig. 8). These additional vortices are, however, restricted to a small range at the pressure side of the channel. Therefore they do not affect the main flow velocity distribution, the pressure loss and heat transfer characteristics.

The influence of the channel height b assuming a constant width a on the pressure loss is demonstrated in Fig. 9. Herein the pressure gradient C_p is plotted versus the aspect ratio λ for several rotation numbers Ro. For large values of λ all curves

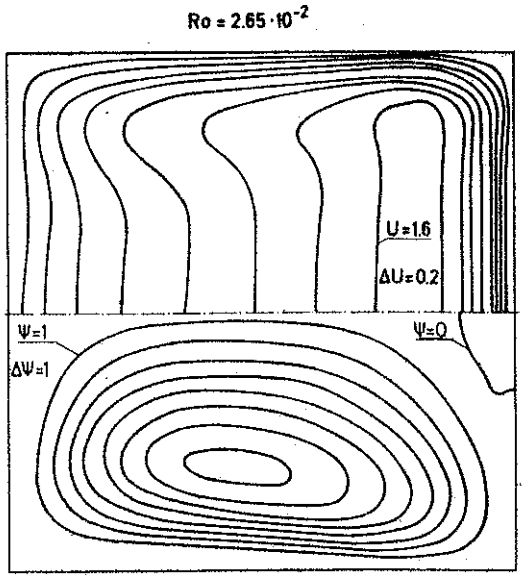

FIG. 8. Lines of constant main flow velocity, upper half, and stream function contours, lower half of the cross section, for a square channel with Re=1000 and Ro=$2.65 \cdot 10^{-2}$.

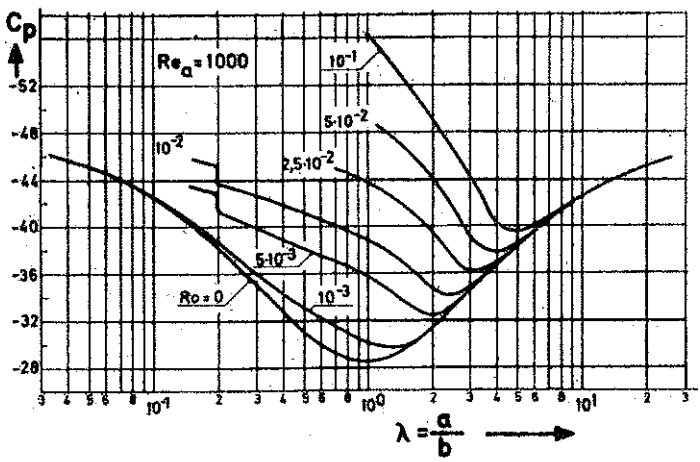

FIG. 9. Pressure gradient C_p versus aspect ratio λ for Re_a=1000 with the Rotation number Ro as a parameter.

reach the asymptotic solution for Ro=0 because the excitation of the secondary flow diminishes.

$$\lim_{\lambda\to\infty}(De\,D\,\lambda)=0, \quad \mathrm{Ro}=\mathrm{const}. \tag{3.2}$$

In this limiting case one obtains the creeping flow without any secondary flow motion, because the Reynolds number $\mathrm{Re}=\mathrm{Re}_a D$ itself also runs to zero. For very small aspect ratios λ where the Reynolds number reach its maximum value $\mathrm{Re}(\lambda=0)=2\mathrm{Re}_a$ and the excitation become zero again

$$\lim_{\lambda\to 0}(\mathrm{De}\,D\,\lambda)=0, \quad \mathrm{Ro}=\mathrm{const}, \tag{3.3}$$

we obtain the second limiting case of an approximately plane flow with diminishing secondary flow. Then the profile of the main flow is independent of Z and can be expressed as a function of Y only:

$$\text{plane flow: } U'(Y)=6(Y-Y^2). \tag{3.4}$$

Hence, the pressure gradient C_p for $\lambda=0$ becomes

$$\lim_{\lambda\to 0} C_p=\lim_{\lambda\to 0}\left(D^2\frac{\partial^2 U}{\partial Y^2}\right)_{Y=0}=-48, \tag{3.5}$$

which is confirmed by the numerical results shown in Fig. 9. Furthermore it should be noticed that the pressure gradient of the channel flow for $\lambda\to 0$ is four times greater than the pressure gradient of plane flow. Starting from a small channel height b, that means large aspect ratios, the pressure gradient first decreases, reaches an absolute minimum and then increases with increasing b. Following the curves for $\mathrm{Ro}=5\cdot 10^{-3}$ an abrupt jump of the pressure gradient occurs. This effect may be understood looking at the secondary flow pattern. At $\lambda\approx 0.2$ a second pair of fully developed vortices appears (see Fig. 10).

Because these additional vortices are extended to the whole channel width, they strongly affect the main velocity distribution, friction factor and heat transfer data.

3.2. Heat transfer

Similarly to the representation of pressure loss the increase of heat transfer due to rotation may also be correlated to the Dean number De (see Fig. 11).

For De>10 the temperature gradient C_θ strongly increases with increasing rotation while the heat transfer at the pressure side is higher than the heat transfer at the suction side of the channel. The increase of heat transfer is greater than the increase of pressure loss. At $\mathrm{Ro}=10^{-2}$ and De=100 respectively the increase of heat transfer is about 150%.

Assuming a constant channel width a the influence of the channel height b on the heat transfer was investigated (see Fig. 12).

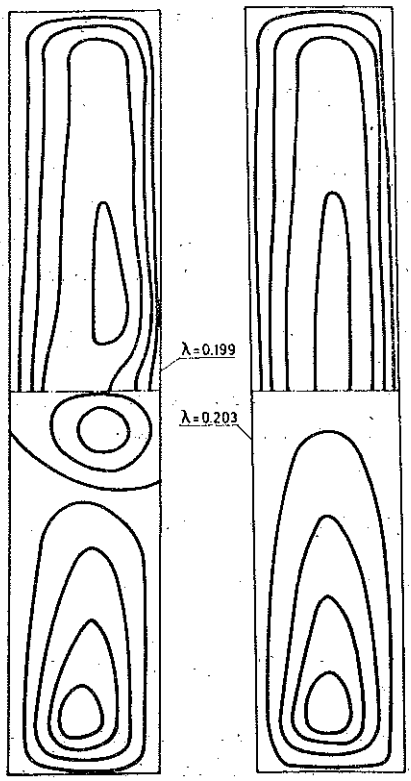

FIG. 10. Lines of constant main velocity, upper half, and stream function contours, lower half of the cross section, for $Re_a=1000$, $Ro=5\cdot10^{-3}$ and two geometries $\lambda=0.203$ and 0.199.

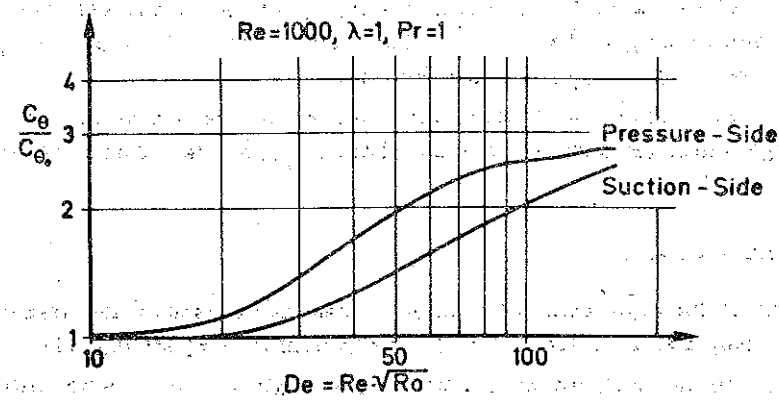

FIG. 11. Increase of temperature gradient C_θ/C_{θ_0} due to rotation versus Dean number for Re=1000, $\lambda=1$ and Pr=1.

Considering the curve for Ro=0 two limiting cases are to be differed. First, for very small values of λ the height b goes to infinity and an approximately plane flow can be supposed. Taking into account the corresponding main velocity profile

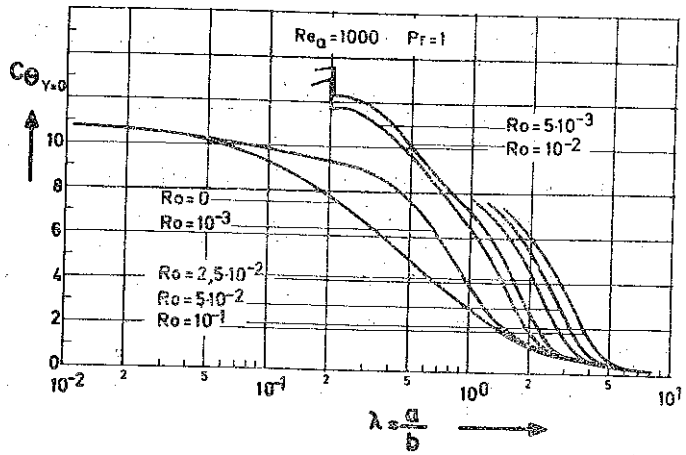

FIG. 12. Temperature gradient C_θ versus aspect ratio λ for $Re_a=1000$ and $Pr=1$ with the Rotation number Ro as a parameter considering heat transfer at pressure side $Y=0$.

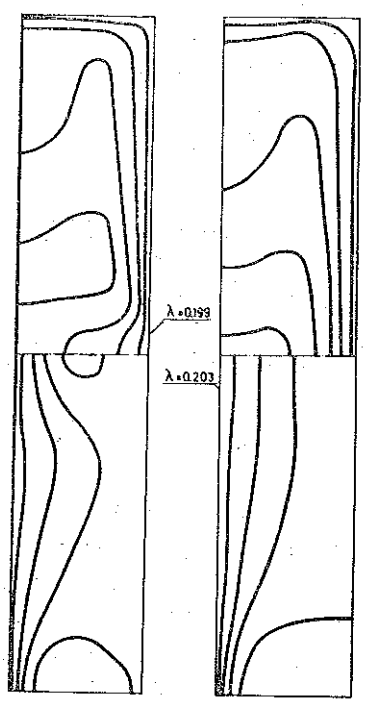

FIG. 13. Lines of constant temperature considering heat transfer at pressure side, upper half, and at suction side, lower half of the channel for $Re_a=1000$, $Ro=5\cdot10^{-3}$ and two geometries $\lambda=0.203$ and 0.119.

(3.4) the simplified energy equation $-Pr\cdot U=D^2\,\partial^2\theta/\partial Y^2$ can be integrated analytically and yields the following temperature profile:

$$\text{(3.6)} \qquad \text{plane flow: } \theta(Y)=\frac{Pr}{4}\left(Y-Y^3+\frac{1}{4}Y^4\right).$$

Hence the temperature gradient C_θ can be evaluated using Eq. (2.3)

$$\lim_{\lambda\to 0} C_\theta = \lim_{\lambda\to 0}\left(\frac{D^2}{\mathrm{Pr}}\cdot\frac{12D^2}{-C_p}\cdot\frac{20}{7}\right)=\frac{80}{7}=11.43\,. \tag{3.7}$$

The numerical results show a good agreement with these theoretical considerations. Second, considering very large aspect ratios the height b of the channel tends to zero so that no heat can be transferred, $C_\theta=0$. For $\mathrm{Ro}>0$ the temperature gradient C_θ strongly increases with increasing channel height b and decreasing aspect ratio λ respectively. Similarly to the jump of the pressure gradient at $\lambda\approx 0.2$ the additional vortices change the flow pattern and temperature distribution (see Fig. 13), and therefore also cause a sudden increase of the temperature gradient C_θ.

3.3. Efficiency factor

Comparing the effect of rotation both on the pressure loss and the heat transfer, the numerical investigations clearly show that the temperature gradient is affected in a stronger way than the pressure gradient. In Fig. 14 the increase of the efficiency factor $G\ddot{u}/G\ddot{u}_0$ is plotted against the Dean number De.

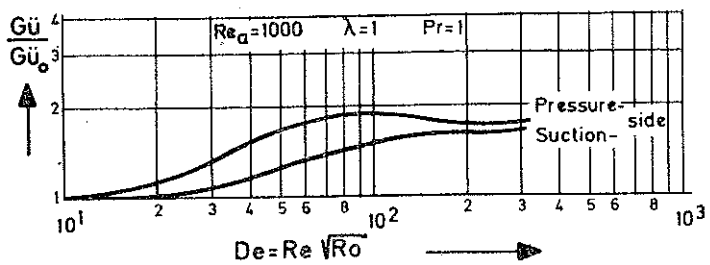

FIG. 14. Increase of the efficiency factor $G\ddot{u}/G\ddot{u}_0$ due to rotation versus Dean number De for $\mathrm{Re}_a=1000$, $\lambda=1$ and $\mathrm{Pr}=1$.

The results point out that the efficiency factor $G\ddot{u}$ increases with increasing rotation. Considering heat transfer at the pressure side $G\ddot{u}$ is greater than $G\ddot{u}$ heating the suction side of the channel. At $\mathrm{De}\approx 100$ the improvement of the efficiency factor reaches its maximum value and is about 100%.

In Fig. 15 the product of the Eckert number Ec and the efficiency factor $G\ddot{u}$ considering heat transfer at the pressure side $Y=0$ is plotted against the aspect ratio λ with the Rotation number Ro as a parameter. Corresponding to the estimation of C_p and C_θ at $\lambda=0$ here one obtains

$$\lim_{\lambda\to 0}(\mathrm{Ec}\cdot G\ddot{u})=\lim_{\lambda\to 0}\left(\frac{C_\theta}{C_p}\right)=0.238\,. \tag{3.8}$$

Considering very a large value of λ, the ratio C_θ/C_p runs to zero, $\mathrm{Ec}\cdot G\ddot{u}=0$. In the intermediate range the efficiency factor may be improved remarkably by rotation. Supposing a geometry $\lambda=3$ the improvement is about 400%.

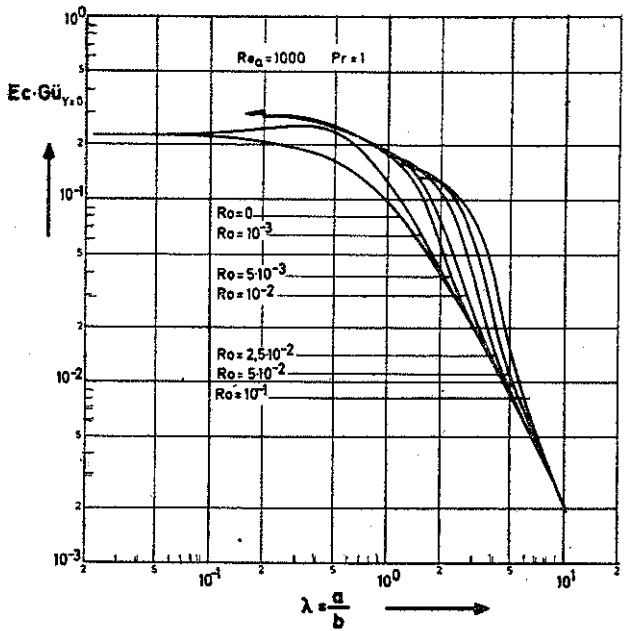

FIG. 15. Product $Ec\ G\ddot{u}_{Y=0}$ versus aspect ratio λ considering heat transfer at pressure side for Re_a=1000 and Pr=1.

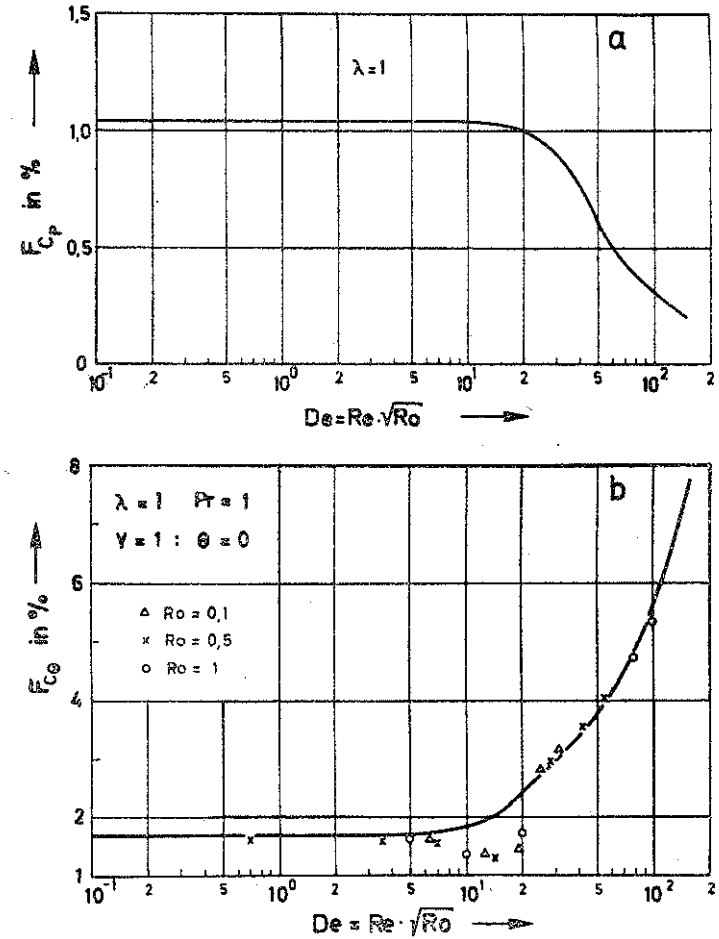

FIG. 16. Numerical errors F_{c_p} and F_c versus Dean number De for λ=1 and Pr=1.

3.4. *Numerical errors*

Assuming constant mesh sizes the numerical errors F_{C_p} and F_{C_θ} primarily depend on the Reynolds number Re and Rotation number Ro. Similarly to the numerical solution C_P and C_θ the numerical errors may be correlated to the Dean number De. For $\mathrm{Ro} < 0.1$ all curves coincide to a single curve (see Fig. 16). In the range of Dean numbers investigated $\mathrm{De} \lesssim 170$ the relative numerical errors F_{C_p} computing the axial momentum equation are less than 1.1% and F_{C_θ} calculating the energy equation reaches a maximum value of 8%.

4. Concluding remarks

The numerical solution procedure will be extended to higher values of the Dean number. Furthermore the steady fully-developed flow field and temperature field in curved rotating channels will be investigated.

References

1. W. R. Dean, *Note of the motion of fluid in a curved pipe*, Phil. Magazine, **4**, 1927.
2. H. Ludwieg, *Die ausgebildete Kanalströmung in einem rotierenden System*, Ing. Archiv, **19**, 1951.
3. K. C. Cheng, Ran-Chaulin and Jenn-Wuu Ou, *Fully developed laminar flow in curved rectangular channels*, J. of Fluids Engineer., **1**, 98, 1976.
4. R. Schilling and R. Simon, *Berechnung der ausgebildeten Strömung in gekrümmten Kanälen mit rechteckigem Querschnitt*, Recent Development in Theoretical and Experimental Fluid Mechanics, Springer Verlag 1979.
5. R. Shilling, *Berechnung der ausgebildeten Strömung in rotierenden Kanälen mit rechteckigem Querschnitt*, ZAMM, **59**, 1979.
6. Y. Mori and Y. Uchida, *Study on forced convective heat transfer in curved square channel*, Trans. Japan Soc. of Mech. Eng., **33**, 1967.
7. K. C. Cheng and M. Akigama, *Laminar forced convection heat transfer in curved rectangular channels*, Int. J. of Heat and Mass Transfer, **13**, 1979.
8. R. Schilling and H. Marcinowski, *Untersuchung des Druckverlustes und des Wärmeüberganges in rotierenden Kanälen mit rechteckigem Querschnitt*, Recent Development in Theoretical and Experimental Fluid Mechanics, Springer Verlag, 1979.
9. L. Trefethen, *Fluid flow in radial rotating tubes*, 9 Congr. Intern. Mech. Appl., Univ. Bruxelles, **2**, 1957.
10. H. Ito and K. Nanbu, *Flow in rotating straight pipes of circular cross section*, Trans. ASME, 1971.

Streszczenie

NUMERYCZNE WYZNACZANIE SPADKU CIŚNIENIA I WYMUSZONEJ KONWEKCJI CIEPŁA W KANAŁACH WIRUJĄCYCH O DOWOLNYM PRZEKROJU PROSTOKĄTNYM

Za pomocą metody różnic skończonych rozważa się pole przepływu laminarnego oraz temperatury w prostoliniowych kanałach wirujących o przekroju prostokątnym. Z rozwiązania równań Naviera–Stokesa i energii wyznacza się spadek ciśnienia, pole przepływu ciepła i wydajność jako funkcje liczby Reynoldsa, obrotów i wydłużenie. Wyniki liczbowe są zgodne z istniejącymi danymi eksperymentalnymi.

Резюме

ЧИСЛЕННОЕ ОПРЕДЕЛЕНИЕ ПЕРЕПАГА ДАВЛЕНИЯ И ВЫНУЖДЕННОЙ КОННЕКЦИИ ТЕПЛА ВО ВРАЩАЮЩИХСЯ КАНАЛАХ С ПРОИЗВОЛЬНЫМ КВАДРАТНЫМ СЕЧЕНИЕМ

С помощью метода конечных разностей рассматривается поле ламинарного течения, а также температуры в простолинейных вращающихся каналах с квадратным сечением. С помощью решения уравнений Навы-Стокса и энергии определяется перепад давления, поле течения и производительность как функция числа Рейнольдся, оборотов и удлинения. Численные результаты совпадают с существующими экспериментальными данными.

LEHRSTUHL FÜR STRÖMUNGSMASCHINEN
UNIVERSITÄT KARLSRUHE, BRD.

Received October 25, 1979.